In vivo amelioration of endogenous antitumor autoantibodies via low-dose P_4N through the LTA4H/activin A/BAFF pathway

Yu-Ling Lin[a,b], Nu-Man Tsai[c,d], Cheng-Hao Hsieh[a], Shu-Yi Ho[a], Jung Chang[a], Hsin-Yi Wu[e], Ming-Hua Hsu[f], Chia-Ching Chang[a], Kuang-Wen Liao[a,e,g,1,2], Tiffany L. B. Jackson[h], David E. Mold[h], and Ru Chih C. Huang[a,h,1,2]

[a]Department of Biological Science and Technology, National Chiao Tung University, Hsinchu, 30068, Taiwan, Republic of China; [b]Center for Bioinformatics Research, National Chiao Tung University, Hsinchu, 30068, Taiwan, Republic of China; [c]School of Medical Laboratory and Biotechnology, Chung Shan Medical University, Taichung, 40201, Taiwan, Republic of China; [d]Clinical Laboratory, Chung Shan Medical University Hospital, Taichung 40201, Taiwan, Republic of China; [e]Institute of Molecular Medicine and Bioengineering, National Chiao Tung University, Hsinchu, 30068, Taiwan, Republic of China; [f]Nuclear Science & Technology Development Center, National Tsing Hua University, Hsinchu, 30013, Taiwan, Republic of China; [g]Graduate Institute of Medicine, College of Medicine, Kaohsiung Medical University, Kaohsiung, 80708, Taiwan, Republic of China; and [h]Department of Biology, Johns Hopkins University, Baltimore, MD 21218-2685

Edited by Jason G. Cyster, University of California, San Francisco, CA, and approved October 24, 2016 (received for review March 30, 2016)

Cancer progression is associated with the development of antitumor autoantibodies in patients' sera. Although passive treatment with antitumor antibodies has exhibited remarkable therapeutic efficacy, inhibitory effects on tumor progression by endogenous antitumor autoantibodies (EAAs) have been limited. In this study, we show that P_4N, a derivative of the plant lignan nordihydroguaiaretic acid (NDGA), enhanced the production of EAAs and inhibited tumor growth at low noncytotoxic concentrations via its immunoregulatory activity. Intratumoral injection of P_4N improved the quantity and quality of EAAs, and passive transfer of P_4N-induced EAAs dramatically suppressed lung metastasis formation and prolonged the survival of mice inoculated with metastatic CT26 tumor cells. P_4N-induced EAAs specifically recognized two surface antigens, 78-kDa glucose-regulated protein (GRP78) and F1F0 ATP synthase, on the plasma membrane of cancer cells. Additionally, P_4N treatment led to B-cell proliferation, differentiation to plasma cells, and high titers of autoantibody production. By serial induction of autocrine and paracrine signals in monocytes, P_4N increased B-cell proliferation and antibody production via the leukotriene A4 hydrolase (LTA4H)/activin A/B-cell activating factor (BAFF) pathway. This mechanism provides a useful platform for studying and seeking a novel immunomodulator that can be applied in targeting therapy by improving the quantity and quality of the EAAs.

endogenous antitumor autoantibody | P_4N | B-cell proliferation | colorectal cancer | cancer immunotherapy

Colorectal cancer (CRC) is the second most prevalent cancer in the western world and is also rapidly increasing in Asia (1). It is well known that multiple genetic events involved in the development of this disease lead to the generation of tumor-associated antigens (TAAs) against which patients with CRC develop autoantibodies (2). More than 100 TAAs have been identified by these endogenous antitumor autoantibodies (EAAs), including 78-kDa glucose-regulated protein [GRP78, also known as binding Ig protein (BiP)], p53, carcinoembryonic acid (CEA), and mucin 1 (MUC1) (2). The use of these autoantibody signatures as biomarkers in the early detection of CRC has been proposed (3–5). Typically, EAAs have not had a significant effect on tumor elimination, most likely due to immune tolerance induction by the tumor (6, 7). However, extraction of EAAs from the sera of patients with cancer to activate the humoral immune response against some malignant tumors has been considered. A few EAAs selected from patients, such as SC-1 (anti-CD55), PAM-1 [anti–cysteine-rich fibroblast growth factor (anti-CFR1)], and PAT-SM6 (anti-GRP78), act directly against tumors and effectively kill them via antibody-mediated cellular cytotoxicity (8). In addition, a natural human IgM autoantibody (PAT-SM6) selected from patients' sera against the cell surface GRP78 protein provides therapeutic effects for patients with cancer (9, 10). Although the therapeutic effects of EAAs are ill-defined, these studies display their potential for clinical therapy.

Alternatively, passive immune therapeutics composed of antibodies ligated to targeted molecules (11) and directed against tumor growth factors (12) have been used clinically to induce apoptosis of tumor cells directly. Moreover, these passive therapeutic antibodies trigger complement-dependent cytotoxicity (CDC) or antibody-dependent cellular cytotoxicity (ADCC) (12, 13), promote phagocytosis by dendritic cells (DCs) (14), induce cross-talk between immune cells [natural killer (NK) cells and DCs], produce immunomodulatory cytokines (type I and type II interferons) (12), and enhance the cross-presentation of antigen-presenting cells (APCs) for the priming of $CD8^+$ cytotoxic T lymphocytes (CTLs) (12, 14). By these reactions, passive therapeutic antibodies can be effective agents for tumor inhibition. The effectiveness of therapeutic antitumor antibodies portends the potential of enhanced or improved EAAs to function as effective therapeutic entities.

Significance

This study finds that a small-molecule drug (P_4N) is able to inhibit tumor growth by augmentation of endogenous antitumor autoantibodies (EAAs). We show that the enhancement of EAA activity by P_4N is mediated through activation of the leukotriene A4 hydrolase (LTA4H)/activin A/B-cell activating factor (BAFF) pathway, revealing a valuable method for developing new immune modulators of tumor growth via humoral immunity. Typically, the effects of the humoral response on tumor inhibition are modest; however, the results of this study demonstrate that by removing the impediment to cancer cell destruction posed by low-activity autoantibodies, the realization of new, more potent immunotherapies for cancer treatment may be possible.

Author contributions: Y.-L.L., K.-W.L., and R.C.C.H. designed research; Y.-L.L., N.-M.T., C.-H.H., S.-Y.H., J.C., H.-Y.W., C.-C.C., T.L.B.J., and D.E.M. performed research; M.-H.H. and R.C.C.H. contributed new reagents/analytic tools; Y.-L.L. analyzed data; and Y.-L.L., K.-W.L., D.E.M., and R.C.C.H. wrote the paper.

The authors declare no conflict of interest.

This article is a PNAS Direct Submission.

Freely available online through the PNAS open access option.

Data deposition: Gene Expression Profiling has been deposited and published in Gene Expression Omnibus at National Center for Biotechnology Information (accession no. GSE89659).

[1]K.-W.L. and R.C.C.H. contributed equally to this work.

[2]To whom correspondence may be addressed. Email: rhuang@jhu.edu or liaonms@mail.nctu.edu.tw.

This article contains supporting information online at www.pnas.org/lookup/suppl/doi:10.1073/pnas.1604752113/-/DCSupplemental.

Recently, low-dose chemotherapy (metronomic chemotherapy) has been shown to induce an antitumor immune response and enhance the efficacy of cancer therapy. For example, the anti-microtubule taxanes (paclitaxel and docetaxel) were found to trigger the production of cytokines by macrophages to activate other immune cells, such as DCs (15), NK cells (16), and CTLs, against tumors (16, 17). Paclitaxel also reduced the number of regulatory T (Treg) cells and myeloid-derived suppressor cells (MDSCs), and led to the augmentation of the functions of CD4 and CD8 T cells (16, 17). In other cases, DNA alkylating agents, such as cyclophosphamide and mafosfamide, in low doses selectively depleted Treg cells (18, 19), caused an increase in effector T cells (Teff)/Treg cell ratios via up-regulation of the T helper (Th) 17 pathway (20), and improved the outcome of tumor vaccinations against cancer (21–23). Furthermore, doxorubicin, mitomycin C, vinblastine, and methotrexate in low doses have been found to up-regulate DC maturation, antigen processing, and antigen presentation, which led to synergistic antitumor effects of low-dose chemotherapy combined with a DC vaccine (24–26). These various antitumor drugs in low doses can induce cell-mediated immunity against tumors, but they have less of a contribution to humoral immunity. Therefore, they have not been used to raise EAAs against tumor growth in patients.

P_4N, a derivative of nordihydroguaiaretic acid (NDGA), a natural product from the creosote bush, *Larrea tridentate*, is composed of two phenolic rings connected by long and flexible $–CH_2–CH_2–$ linkers to piperidines (27). Like methylated derivatives of NDGA, P_4N has shown noteworthy antivirus and anticancer effects via competition with the transcription factor Sp1 for its DNA-binding site (27, 28). P_4N's parent compound, NDGA, is a potent antioxidant and has been shown to have promising applications in the treatment of multiple diseases, including cardiovascular disease and neurological disorders (29). It also inhibits the growth of various tumors (30), although it is substantially less potent than P_4N (*SI Appendix*, Fig. S1) and likely has a different mechanism of action (28). NDGA has immunoregulatory activities as well. It inhibits 5-lipoxygenase, suppresses the production of leukotriene B4 (LTB4), and activates macrophages (29). The effect of P_4N on immune function is unknown.

In this study, the immunoregulatory activity of low-dose P_4N was investigated. Unlike previously described antitumor drugs, low-dose P_4N contributes to humoral immunity by raising the titers and activities of autoantibodies against GRP78 and F1F0 ATP synthase on the surface of CT26 cells and inducing B-cell proliferation and differentiation of plasma cells. We show that low-dose P_4N induces B-cell proliferation by activating leukotriene A4 hydrolase (LTA4H), thereby enhancing the production of LTB4 and stimulating monocytes to release proinflammatory cytokines. The release of activin A acts as an autocrine signal, stimulating B-cell activating factor (BAFF) production via activation of the ALK4/Smad3 pathway. BAFF then enhances B-cell proliferation and activation.

Results

P_4N-Activated Humoral Immune Response Suppresses Tumor Growth in Vivo. To examine whether low-dose P_4N causes immunoregulatory activity for the suppression of tumor growth, the effects of a single intratumoral injection with 2.5 mg/kg or 5 mg/kg of P_4N into CT26 tumors in BALB/c or nude mice were monitored. Both doses of P_4N significantly inhibited the growth of CT26 tumors in BALB/c mice, but had no effect on the growth of CT26 tumors in the immunodeficient nude mice (Fig. 1*A*). As shown in Fig. 1*B*, $CD8^+$ T-cell depletion attenuated the effect of P_4N-induced tumor inhibition. In contrast, B-cell depletion abolished the effect of P_4N-induced tumor inhibition (Fig. 1*B*). The tumor-suppressive effects of P_4N were not the result of direct cytotoxicity of the drug, because there was no significant difference in tumor growth between P_4N and PBS treatments in the B-cell–depleted mice. These results suggested that a humoral immune response may play a major role in P_4N-induced tumor inhibition.

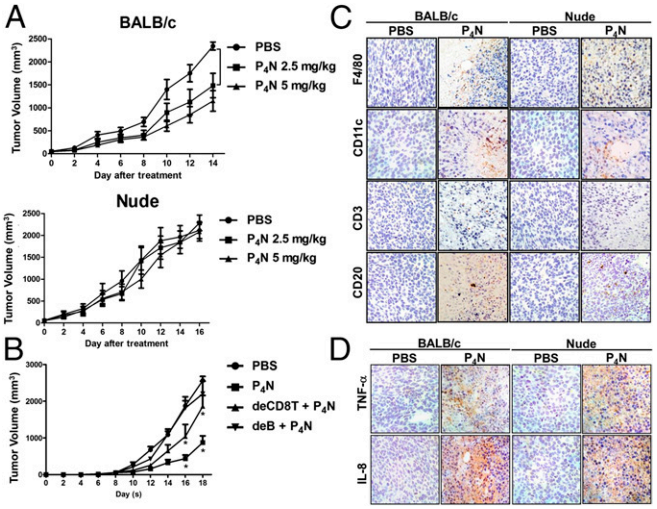

Fig. 1. Antitumor effects of low-dose P_4N in immune-competent and -deficient mice. (*A*) BALB/c ($n = 10$ per group) and nude mice ($n = 10$ per group) bearing CT26 tumors were treated with a single intratumoral injection of 2.5 or 5.0 mg/kg of P_4N. (*B*) B-cell– or $CD8^+$ T-cell–depleted BALB/c mice ($n = 9$ per group) bearing CT26 tumors were treated with 5 mg/kg of P_4N by intratumoral injection every week. Tumor volumes were measured every 2 d after treatment. Significant differences between the P_4N groups and the PBS group were identified and labeled with $*P < 0.05$ and $**P < 0.01$. (*C*) IHC staining was used to monitor the infiltration of macrophages (F4/80), DCs (CD11c), T cells (CD3), and B cells (CD20) in the tumor area after a single intratumoral injection of PBS or 5 mg/kg of P_4N. The photographs are representative of the mice killed on day 7 after the treatments. (*D*) Expression of TNF-α and IL-8 in the tumors was also observed by IHC staining. (Magnification: *C* and *D*, 400×.)

Using an immunohistochemistry (IHC) assay, it was shown that P_4N treatments led to the infiltration of immune cells, such as macrophages, DCs, and T or B cells, into the tumor area (Fig. 1*C*). There was no significant difference between the two mouse strains in terms of the levels of macrophages and DCs in the tumors, but the levels of T and B cells in the tumors were higher in BALB/c mice than in nude mice (*SI Appendix*, Fig. S2). In addition, it was found that P_4N treatments enhanced the expression levels of TNF-α and IL-8 in both strains of mice (Fig. 1*D*). Taken together, these results indicate that low-dose P_4N elicits certain immune responses in tumors, but only suppresses tumor growth in BALB/c mice, where adaptive immunity may play an important role.

To determine whether humoral immunity is involved in the antitumor activity of low-dose P_4N, sera isolated from P_4N- or vehicle (PBS)-treated CT26 tumor-bearing mice were passively transferred into BALB/c mice inoculated with metastatic CT26 cells. Within 18 d after tumor cell injection, untreated mice developed lung metastases, with metastatic nodules surrounding the lungs. Administration with antisera derived from PBS-treated mice decreased the number of metastatic nodules and the total weight of the lungs (Fig. 2 *A* and *B*). P_4N-derived antisera displayed an even stronger effect, dramatically inhibiting tumor colonization, as evidenced by the nearly complete lack of metastatic nodules and total lung weights approaching the total lung weights of normal mice. All mice treated with P_4N antisera survived more than 60 d, a survival time threefold the survival time of the control groups (Fig. 2*C*). These results suggested that the inhibition of tumor colonization by P_4N antisera might be the result of P_4N-induced EAAs in the sera.

The Effect of P_4N on Production and Activity of Antitumor Autoantibodies. To eliminate the influence of T cells, the antisera were injected into CT26 tumor-containing immunodeficient mice. P_4N antisera still significantly suppressed tumor growth in these mice, whereas PBS antisera had no significant effect on

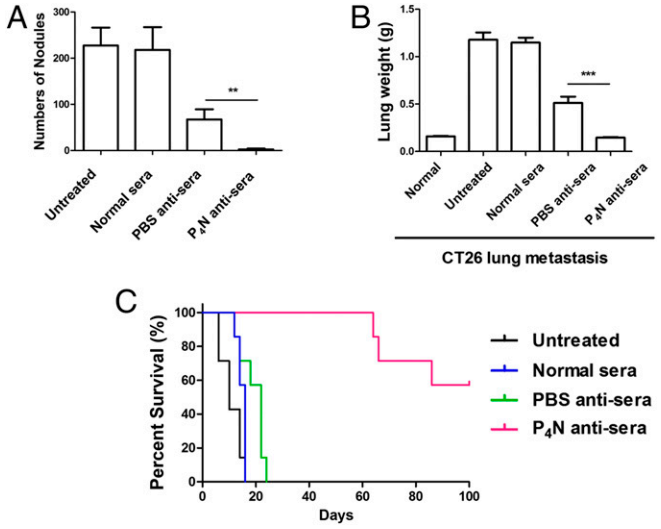

Fig. 2. Effect of P_4N-induced antisera on the formation of pulmonary tumor nodules. (*A*) Number of lung metastases in each group was counted and expressed as the mean ± SD (n = 5 per group). Mean lung weight (*B*) and mean survival rate (*C*) of mice in each group (n = 7 per group) were calculated and plotted. Data were collected from two independent experiments. Significant differences between the P_4N antisera group and the PBS antisera group were determined and labeled with $^{**}P < 0.01$ and $^{***}P < 0.001$.

tumor growth (Fig. 3*A*). Characterization of the antisera revealed that the titers of specific anti-CT26 antibodies in P_4N antisera were higher than in PBS antisera, regardless of the time of harvest (Fig. 3*B*), and the major classes of increased antibodies in P_4N antisera were IgG1 and IgA (Fig. 3*C*). Like normal mouse sera, PBS antisera only somewhat recognized the tumor cells in CT26 tumor tissue; however, the P_4N antisera displayed a strong binding affinity for the cells (Fig. 3*D*).

Of interest are the antigens that are recognized by EAAs in sera derived from tumor-bearing mice. Fig. 3*E* shows that although both antisera recognized surface antigens on CT26 cells, P_4N antisera was more proficient than PBS antisera. By confocal microscopy, the autoantibody-bound antigens on the plasma membrane were distributed in a speckled pattern, implying their presence in complexes associated with other cell surface proteins (Fig. 3*F*). A Western blot assay determined that the autoantibodies in the antisera recognized 78-kDa and 55-kDa proteins on the membranes of CT26 cells (Fig. 3*G*). The antigen profile on the cell membrane was further delineated by co-immunoprecipitation of a membrane protein extract with the antisera. Proteins of 78 kDa and 55 kDa were precipitated, along with at least six other proteins. The 78-kDa and 55-kDa proteins were identified by ultra performance liquid chromatography (UPLC) high-resolution tandem mass spectrometry (HRMS/MS) as GRP78 and F1F0 ATP synthase, respectively (*SI Appendix*, Fig. S3*A*).

To determine if the antitumor effects of P_4N antisera are mediated by antibodies directed at these two antigens, GRP78- and ATP synthase-specific peptides (*SI Appendix*, Fig. S3*B*) were tested for their ability to neutralize the cytotoxic activities of the P_4N-induced antitumor autoantibodies. First, it was established that P_4N antisera is cytotoxic to CT26 cells in culture (Fig. 3*H*) and that the peptides were able to bind to the P_4N antisera (*SI Appendix*, Fig. S3*C*). Subsequently, the cytotoxic effects of P_4N antisera combined with GRP78- and ATP synthase-specific peptides were analyzed. The results (Fig. 3*I*) showed that the peptides decreased the cytotoxicity of P_4N antisera, confirming that P_4N treatments enhance the production and activity of anti-GRP78 and anti-F1F0 ATP synthase autoantibodies that promote CT26 tumor inhibition.

The Effect of Low-Dose P_4N on B-Cell Proliferation and Ig Regulation. The immune modulation effects of P_4N were investigated by testing the ability of low-dose P_4N to affect the proliferation of human peripheral blood mononuclear cells (PBMCs) in vitro. As shown in *SI Appendix*, Fig. S4*A*, PBMC proliferation, as measured by the MTT (3-(4,5-dimethyl-2-thiazolyl)-2,5-diphenyl-2-H-tetrazolium bromide) colorimetric assay, was increased by 10–40%, depending on the dose of P_4N. Flow cytometry analysis of B cells from six healthy individuals showed that P_4N significantly increased the proliferation of the B-cell population in human PBMCs (*SI Appendix*, Fig. S4*B*). B-cell proliferation was also analyzed in mouse splenocytes, and a similar P_4N-induced increased in total splenic B-cell proliferation was observed (*SI Appendix*, Fig. S4*C*). Upon further analysis, it was determined that the increase in total B-cell proliferation was the result of the proliferation of naive B cells. P_4N had no effect on the number of activated B cells in the absence of antigen stimulation. These results suggest that P_4N treatments have similar effects in mice and humans.

Enhanced green fluorescent protein (EGFP) was used as a model antigen to monitor specific antibody production and B-cell differentiation after antigen stimulation. BALB/c mice were immunized and boosted using i.p. injections with the EGFP antigen combined with one-time or three-times weekly P_4N injections. P_4N dramatically enhanced total specific anti-EGFP Ig production, especially when EGFP was combined with P_4N injections three times a week (*SI Appendix*, Fig. S4*D*). In addition, immunization plus P_4N significantly increased IgG1, IgG2b, and IgA production (*SI Appendix*, Fig. S4*E*). These results indicate that P_4N promotes specific antibody production by up-regulating the Th2-mediated immune response. Analysis of B-cell types revealed that both memory and plasma cells were increased after EGFP immunization (*SI Appendix*, Fig. S4*F*). EGFP immunization combined with P_4N resulted in an even larger stimulation of B-cell differentiation to plasma cells, suggesting that P_4N treatment could promote enhanced antibody production.

Role of Monocytes and Cytokine Expression in P_4N-Induced B-Cell Proliferation. P_4N did not induce the proliferation of isolated T cells or B cells, yet it increased the proliferation of T-cell–depleted PBMCs (*SI Appendix*, Fig. S5), indicating that P_4N-induced B-cell proliferation may require the presence of monocytes. Examination of the cytokine profiles of PBMCs after P_4N treatment showed that the levels of proinflammatory cytokines (TNF-α, IL-1β, and IL-6) and chemokines (IL-8, IP-10, MIP-1α, MIP-1β, and RANTES) were significantly increased after P_4N treatment (*SI Appendix*, Fig. S6). Using a Bio-Plex assay for human cytokines to analyze THP-1 monocyte-like cells, it was determined that after P_4N treatment, the THP-1 cells increased the expression of proinflammatory cytokines and chemokines, similar to PBMCs (Fig. 4*A*). Moreover, P_4N rapidly induced TNF-α and IL-1β expression in THP-1 monocytes within 4 h, and then stimulated IL-8 release after 8 h (*SI Appendix*, Fig. S7), suggesting that P_4N's effect on monocytes results in a cascade of increased cytokines and chemokines.

Another cell type in the peripheral tissue that is able to stimulate B-cell proliferation is the DC. The effects of P_4N on mouse bone marrow-derived (mBM) DCs were analyzed, and the results showed P_4N did not induce cell proliferation of mBM-DCs or increase their expression of BAFF (*SI Appendix*, Fig. S8 *A* and *B*). LTA4A expression was increased in the monocyte/macrophage population, but not in mBM-DCs (*SI Appendix*, Fig. S8*C*).

To determine the factors involved in P_4N-induced B-cell proliferation, the gene expression pattern of monocytes treated with P_4N was analyzed by cDNA microarray. The results of this analysis revealed 26 up-regulated genes of cytokine–cytokine interaction [Kyoto Encyclopedia of Genes and Genomes (KEGG) pathway] and 10 up-regulated genes of growth factor activity [Gene Ontology (GO): 0008083] in THP-1 cells following P_4N treatment (Fig. 4*B*). Based on these results, the factor most

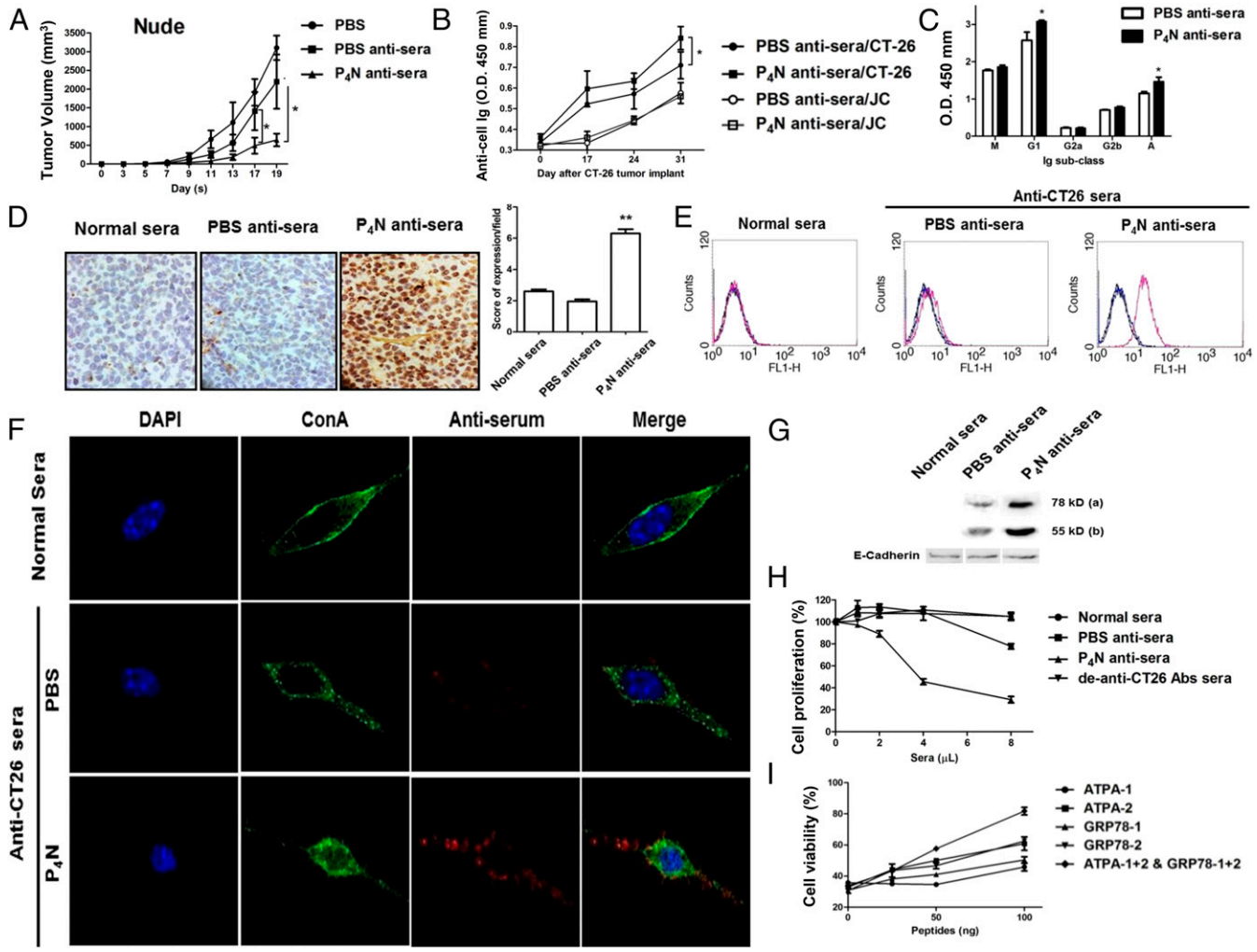

Fig. 3. Antitumor effect of P_4N-induced antiserum in immunodeficient mice and the target antigens of the antiserum. (*A*) Nude mice bearing CT26 cell tumors ($n = 5$ per group) were treated with 100 μL of PBS, PBS antisera, or P_4N antisera weekly. Tumor volumes were measured every 2 d after treatment. (*B*) Titers of specific anti-CT26 or JC cell antibodies for the PBS antisera or P_4N antisera on days 0, 17, 24, and 31 were measured. (*C*) Effects of P_4N on the changes in the isotypes of specific anti-CT26 cell antibodies were examined. The titers of these antisera (1,600× dilution) were measured for IgM, IgG1, IgG2a, IgG2b, or IgA. (*D*) IHC analysis of antisera bound to tumor antigens on the surface of CT26. Color development by HRP-conjugated anti-mouse antibodies indicates the antisera antibody. (*E*) Antisera binding to tumor antigens on the surface of CT26 cells was indirectly detected with FITC-conjugated goat anti-mouse IgG antibody. (*F*) Subcellular location of antigens recognized by the antisera was monitored by confocal microscopy. Alexa Fluor 568-conjugated anti-mouse Ig antibodies were used to display the presence of antisera (red). Alexa Fluor 488-Con A and DAPI were used to indicate the cell membrane (green) and the cell nucleus (blue), respectively. (*G*) Normal sera, PBS antisera, or P_4N anti-sera were used to probe Western blots of membrane proteins of extracted from CT26 cells. Two bands of 78 kDa and 55 kDa were visualized: E-cadherin proteins were used as a loading control. For all results, significant differences between the P_4N antisera group and the PBS antisera group were calculated and labeled with $*P < 0.05$. (*H*) Proliferation of CT26 cells treated with 1, 2, 4, or 8 μL of sera was analyzed by MTT assay. To create de–anti-CT26 antibody sera, the anti-CT26 autoantibodies from P_4N antisera were presubtracted by CT26 cell binding. The data are reported as the proliferation index. Significant differences between the P_4N-treated groups and the untreated group were indicated by $*P < 0.05$ ($n = 5$). (*I*) Cytotoxicity of P_4N antisera after neutralization with ATPA and GRP78 peptides. (Magnification: *C* and *F*, 400×.)

capable of activating B cells without antigen stimulation, BAFF (TNFSF13B), was chosen for further study, along with activin A (INHBA), because it is associated with BAFF expression.

Effect of P_4N-Induced Inflammatory Monocytes on Activin A and BAFF Expression. It has been reported that inflammatory monocytes markedly enhance the production of activin A, which can stimulate APCs to express BAFF (31). In accordance with these reports, we observed that low-dose P_4N induced human PBMCs to increase their gene expression and protein production of activin A and BAFF (Fig. 5*A*) in a dose-dependent manner (Fig. 5*B*). P_4N up-regulated mRNA expression of activin A at 2 h, whereas BAFF expression was elevated at 8 h (Fig. 5*C*). Similar results were obtained in mouse splenocytes (*SI Appendix*, Fig. S9). These results imply that activin A release from P_4N-treated monocytes stimulates the expression of BAFF.

Involvement of the ALK4/Smad3 Pathway in Activin A-Induced BAFF Expression. The pathways involved in activin A-induced BAFF expression after treatment with P_4N were delineated through the use of SB431542, (an ALK4 inhibitor), A83-01 (an ALK4 inhibitor), SIS3 (a Smad3 inhibitor), SB203580 (a p38 inhibitor), and PD98059 (an ERK inhibitor). Inhibitors SB431542, A83-01, and SIS3 significantly reduced BAFF gene and protein expression, whereas inhibitors SB203580 and PD98059 had fewer effects, suggesting that the ALK4/Smad3 pathway mediates the activin A-induced expression of BAFF (Fig. 5 *D* and *E*). Furthermore, conditioned medium from THP-1 cells treated with P_4N increased the proliferation of B cells, whereas conditioned medium from THP-1 cells treated with P_4N and the inhibitors SB431542, A83-01, or SIS3 lost its activity (Fig. 5*F*). These results indicate that P_4N-induced B-cell proliferation is likely due

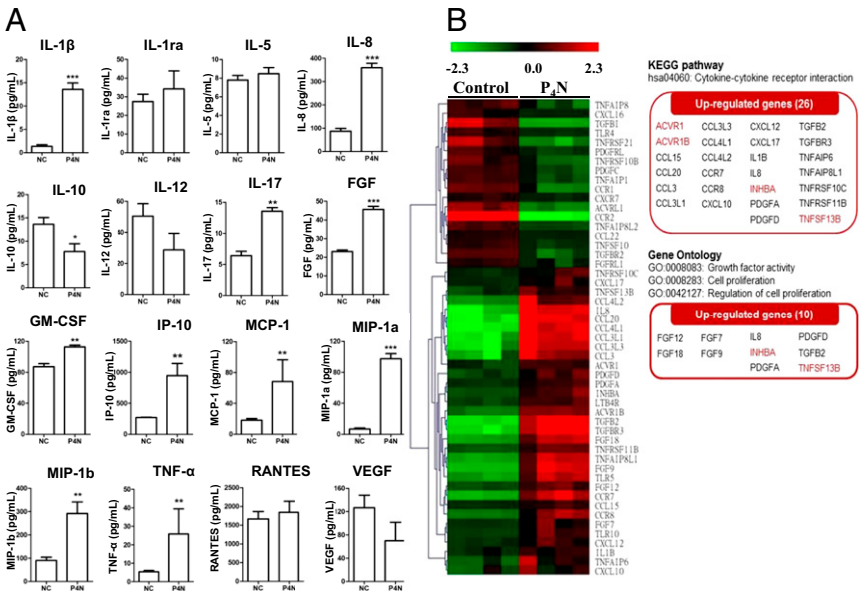

Fig. 4. Cytokine/chemokine and gene expression profiles of P_4N-treated THP-1 cells. (*A*) THP-1 cells were treated with 3 μM P_4N or the vehicle control (NC) for 24 h. Supernatants were collected and analyzed using the Bio-Plex assay for human cytokines. Shown are the concentrations of 27 human cytokines for each treatment from three independent experiments. The levels of IL-2, IL-4, IL-6, IL-7, IL-9, IL13, IL-15, eotaxin, G-CSF, IFN-γ, and PDGF-bb were undetectable. (*B*) Gene expression profiling and analysis. The cDNA microarrays probed with mRNA from untreated or P_4N-treated cells were analyzed, and 26 up-regulated genes involved in cytokine–cytokine interaction and 10 up-regulated genes involved in cell proliferation are highlighted (KEGG pathway, GO panels).

to the action of BAFF that is induced by activin A through the ALK4/Smad3 pathway, Furthermore direct inhibition of activin A or BAFF by specific antibodies abolished the P_4N-induced proliferation of isolated B cells (Fig. 5 *G* and H).

The effect of P_4N treatment on M1/M2 macrophage polarization was assessed by evaluating the mRNA expression of *CD80* (M1) and *CD163* (M2) in human macrophages by RT-PCR. The results showed that P_4N treatments increased the expression of both *CD80* and *CD163* (*SI Appendix*, Fig. S10*A*). In P4N-treated CT26 tumors, the expression of F4/80 (total macrophages), CD68 (M1), and CD163 (M2), as determined by IHC staining, was also increased in a time-dependent manner (*SI Appendix*, Fig. S10*B*).

P_4N Activation of LTA4H and Regulation of Monocyte Inflammation. Next, we sought to determine the molecular targets of P_4N that mediate the response observed in this study. Docking analysis using Swiss Target Prediction and iGEMDOCK software identified the enzyme LTA4H as a potential target of P_4N. P_4N docked at a noncatalytic site of LTA4H compared with the small-molecule active site inhibitor RB3021 (Fig. 6*A*). P_4N also increased the synthesis of the proinflammatory mediator LTB4, a step catalyzed by LTA4H (32) (Fig. 6*B*). These results indicate that the NDGA-derivative P_4N is an LTA4H activator and not an LTA4H inhibitor like its parent molecule NDGA (33, 34), which docks at the active site (*SI Appendix*, Fig. S11). NDGA has been shown to inhibit growth and proliferation and to induce apoptosis in multiple types of cancer cells in tissue culture, including lung, prostate, gastric, neuroblastoma, and breast cancer, through its effects on a variety of molecular targets (30). The effect of NDGA compared with P_4N on in vivo CT26 tumor growth was examined in this study (*SI Appendix*, Fig. S1*B*), along with HT-29 tumor growth (*SI Appendix*, Fig. S1*A*). Results showed that after 48 h of treatment, P_4N was much more potent in causing cell death than NDGA in both cell lines.

The proinflammatory mediator LTB4 induces the expression of cytokines and chemokines; however, it can also be induced by proinflammatory cytokines and chemokines. We therefore used the LTA4H inhibitor bestatin to distinguish whether P_4N induced the expression of the proinflammatory cytokines and chemokines through LTA4H activation or if it increased the activity of LTA4H through their induction. Fig. 6 *C* and *D* shows that P_4N-induced expression of TNF-α and IL-8 was suppressed by bestatin. Thus, it appears P_4N first activates LTA4H to increase LTB4 production and LTB4 then stimulates the expression of proinflammatory cytokines and chemokines.

Finally, it was discovered that bestatin inhibited the P_4N-induced expression of activin A (Fig. 6*E*), implicating P_4N-activated LTA4H in the monocyte stimulation of the activin A/BAFF pathway. Macrophages act as mediators for stimulating activin A and releasing BAFF to induce B-cell activation. Depletion of macrophages by liposomal clodronate in CT26 tumor-bearing BALB/c mice (*SI Appendix*, Fig. S12) reduced the antitumor effects of P_4N (Fig. 6*F*) and clarified the direct target of P_4N as the macrophage. The effect of bestatin on P_4N-induced slowing of tumor growth was further examined, and the results showed bestatin abolished the P_4N-induced inhibition of tumor growth (Fig. 6*G*) and the expression of P_4N-induced activin A and BAFF (Fig. 6*H*).

Discussion

We report that low concentrations of the antitumor drug P_4N contribute to the growth inhibition of colorectal tumors by enhancing the production of endogenous autoantibodies. P_4N not only enhanced the proliferation of B cells to increase the titers of antibodies in sera (Fig. 3*B*) but also increased the activity of antitumor autoantibodies (*SI Appendix*, Fig. S13). The data presented in Fig. 3*F* revealed that although the titers of antitumor autoantibodies in PBS antisera and P_4N antisera are different, they recognized the same antigens, GRP78 and F1F0 ATP synthase, in the membrane fraction (Fig. 3*G* and *SI Appendix*, Fig. S3*A*), indicating that the better antitumor efficacy of P_4N antisera did not result from new antigen recognition but, instead, resulted from the improvement of the quantity and quality of the EAAs.

Without antigen stimulation, B cells cannot be activated and differentiate into plasma cells. Under these conditions, P_4N causes B-cell proliferation and these proliferative B cells arrest at the naive B-cell stage (*SI Appendix*, Fig. S4 *B* and *C*). With

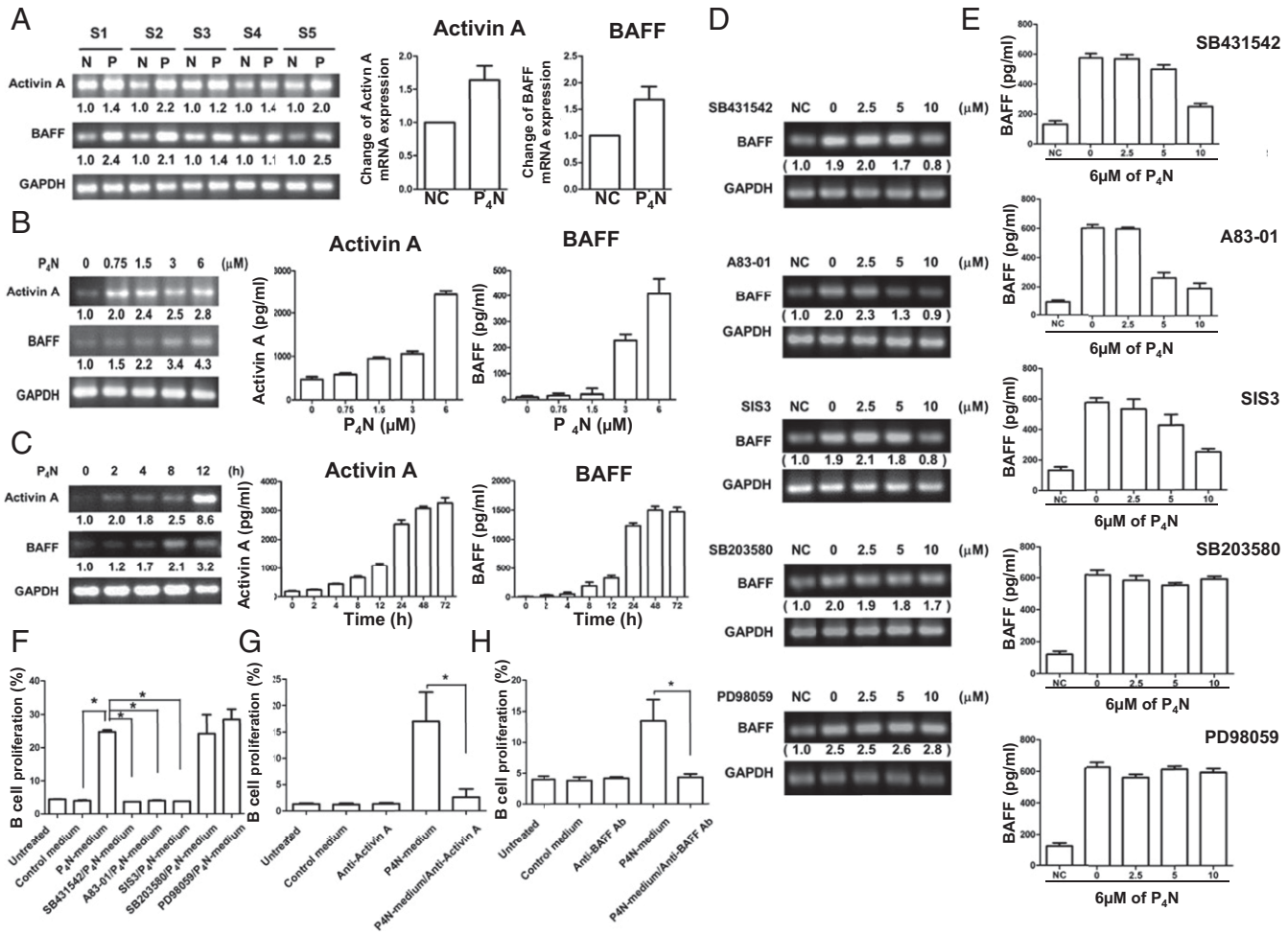

Fig. 5. Expression of activin A/BAFF induced by P_4N treatments. (*A*) P_4N-induced activin A or BAFF expression in human PBMCs as determined by RT-PCR. S1–S5 display different individual blood samples collected from five different human donors. N, no treatment; P, P_4N treatment (3 μM). The change in activin A and BAFF expression (mean of five individuals) relative to the control (NC) is plotted as a histogram. (*B*) Effect of increasing dosages of P_4N for 12 h on mRNA and protein levels of activin A or BAFF in THP-1 cells was analyzed by RT-PCR and ELISA. (*C*) Effect of 6 μM P_4N on mRNA and protein levels of activin A or BAFF in THP-1 cells was determined at a different time period. (*D*) Effect of different inhibitors on activin A-induced BAFF expression was examined. The expression of BAFF mRNA in inhibitor-treated THP-1 cells was determined by RT-PCR (*D*), and BAFF protein secretion was measured by ELISA (*E*). (*F*) Effect of THP-1 condition media on the proliferation of B cells was determined. Media were harvested, in which THP-1 cells were pretreated without inhibitor or with SB431542, A83-01, SIS3, SB203580, or PD98059 and then treated with P_4N for 24 h. The results are expressed as the percentage of viable cells relative to the control (media from untreated THP-1 cells). (*G* and *H*) Anti-activin A and anti-BAFF antibodies blocked THP-1 condition media-induced B-cell proliferation. B cells were treated with P_4N-treated THP-1 media and/or 500 ng of anti-activin A antibody (*G*) or anti-BAFF antibody (*H*) for 30 h. All values are the means of triplicate samples ± SEM. The significant differences in the results of inhibitor and P_4N-treated groups compared with the untreated group are indicated by $^{***}P < 0.001$.

antigen stimulation and the help of $CD4^+$ T cells, B cells that have been induced to proliferate by P_4N will be further activated and differentiate into plasma cells (*SI Appendix*, Fig. S4*F*). Thus, we have proposed that the promotion of EAA production by P_4N treatment is the result of P_4N-accelerated B-cell proliferation and differentiation (*SI Appendix*, Fig. S4 *C* and *F*). This mechanism of action is consistent with the results of P_4N suppression of CT26-derived tumors in mice (Fig. 1 *A* and *B*). In nude mice lacking CD4T cells, immature B cells are unable to mature and differentiate into antibody-producing plasma cells, rendering P_4N ineffective. P_4N retains some antitumor activity in BALB/c mice depleted of CD8T cells, because they still have CD4T cells to help B cells mature and produce antitumor antibodies. Further confirmation of this hypothesis will require additional experiments that examine whether the loss of efficacy seen in B-cell–depleted mice can be rescued by passive transfer of B cells from normal mice or BAFF-deficient mice.

P_4N-induced B-cell proliferation requires BAFF expression (Fig. 5), which is induced by activin A through the ALK4/Smad3 signaling pathway. Similarly, Kim et al. (31) found that activin A can increase BAFF promoter activity and transcription via the ALK4/Smad3 pathway in mice APCs. The finding that P_4N-induced activin A is involved in the stimulation of B-cell proliferation is in accord with the report by Ogawa et al. (35) showing that lipopolysaccharide (LPS)-induced activin A can directly or indirectly increase B-cell proliferation and Ig production. Other reports have shown that activin A induces growth arrest and apoptosis in B-cell–derived cells and hybridomas (36, 37). Activin A-induced apoptosis of B cells relies on the regulation of Bcl-family gene expression (38, 39). Although activin A may cause B-cell apoptosis, BAFF can up-regulate the expression of Bcl-2a1 and down-regulate the expression of BIM for B-cell survival (40). Our data indicate that P_4N-induced B-cell proliferation is the result of BAFF directly stimulating the growth of B cells and preventing activin A-induced B-cell apoptosis.

P_4N improved the quality of the EAA response by inducing Ig class switching from IgM to IgG1 and IgA (Fig. 3*C* and *SI Appendix*, Fig. S4*D*), and it enhanced their binding affinities

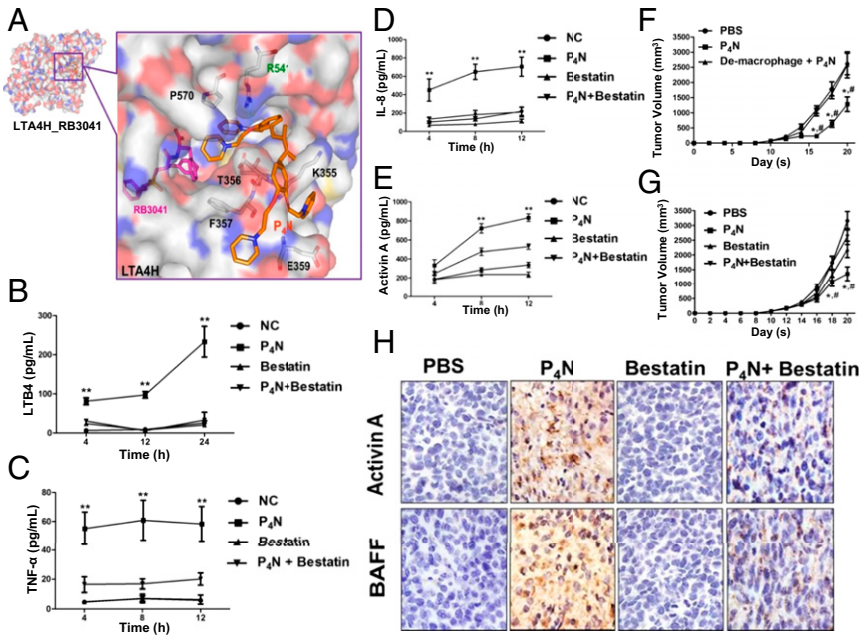

Fig. 6. P_4N directly regulated LTA4H to induce monocyte inflammation. (*A*) P_4N (orange) was docked with LTA4H by iGEMDOCK software (gemdock.life.nctu.edu.tw/dock/igemdock.php). RB3041 (pink) is a small-molecule inhibitor that identifies the active site of LTA4H. The amino acids that potentially interact with P_4N are noted. The effects of P_4N and bestatin on monocytes and their expression of LTB4 (*B*), TNF-α (*C*), IL-8 (*D*), or activin A (*E*) were determined and shown for different times. All values were expressed as the mean ± SEM. $^{**}P < 0.05$ (group P_4N vs. group P_4N + bestatin). (*F*) Macrophage-depleted BALB/c mice ($n = 5$ per group) bearing CT26 tumors were treated with 5 mg/kg of P_4N by intratumoral injection weekly. The significant differences in the results of P_4N-treated groups compared with the untreated group are indicated by $^{*}P < 0.05$; the significant differences in the results of P_4N-treated groups compared with the group of de-macrophage + P_4N are indicated by $^{\#}P < 0.05$. (*G*) Bestatin abolished P_4N-induced inhibition of tumor growth. BALB/c mice bearing CT26 tumors were treated with P_4N (5 mg/kg) and/or bestatin (15 μg/kg) by intratumoral injection weekly. Tumor volumes were measured every 2 d after treatments. The significant differences in the results of P_4N-treated groups compared with the untreated group are indicated by $^{*}P < 0.05$; the significant differences in the results of P_4N-treated groups compared with the group treated with P_4N + bestatin are indicated by $^{\#}P < 0.05$. (*H*) Bestatin suppressed P_4N-induced activin A and BAFF expression. The expression of activin A and BAFF in the tumors was observed by IHC staining. (Magnification: *F* and *H*, 400×.)

(*SI Appendix*, Fig. S13). In the body, IgG1 and IgA easily diffuse into extravascular sites to access antigens and they have a greater efficacy for activating the complement system. Moreover, IgG1 also has a longer $t_{1/2}$ in the blood and can efficiently sensitize NK cells for killing. Thus, the P_4N-induced class switch may be one of the reasons why the P_4N antisera cause more efficient suppression of tumor growth than PBS antisera. Another reason may be that P_4N enhances the process of somatic hypermutation in B cells that causes the antitumor autoantibodies in P_4N antisera to have higher antigen-binding affinities than in PBS antisera, which results in the antitumor autoantibodies being able to bind on the tumor surface stably to trigger more efficient CDC or ADCC. The mechanism of the P_4N-induced Ig class switch and somatic hypermutation involves the activin A-stimulated monocyte release of BAFF via the ALK4/Smad3 pathway (Fig. 5). BAFF up-regulates the expression of the transcription factor Pax5/BSAP, which sequentially increases the transcription of activation-induced cytidine deaminase (AID), an RNA editing enzyme responsible for IgH class switch recombination and somatic hypermutation (41–44). Moreover, class switch recombination must be supported by the splicing of germline transcripts (GLTs), which is involved in recruiting AID to S regions. Activin A also has been reported to induce the class switching of Ig to IgA and IgG2b in B cells through Smad2/3 signaling by up-regulating the expression of Ig germline transcript α (GLTα) and postswitch transcript α (PSTα) (45). By these mechanisms, P_4N could promote B-cell proliferation, differentiation, and function to produce higher titer and higher affinity autoantibodies against tumor growth.

P_4N directly interacted with and activated LTA4H to produce LTB4 (Fig. 6) and induce monocytes to release proinflammatory cytokines, chemokines, and activin A (Fig. 4*A*). Subsequently, activin A stimulated monocytes in an autocrine manner to release BAFF via the ALK4/Smad3 pathway and activate B cells (Fig. 5). According to the docking results, this unique function of P_4N might be a result of its structure (Fig. 6*A*). Unlike NDGA, which inhibits LTB4 production (33), the NDGA derivative P_4N binds differently to LTA4H and acts as an activator and immune mediator to produce more LTB4 (Fig. 6*B*). Once produced, LTB4 is transported out of the cells and binds to LTB4 receptors expressed primarily in leukocytes, and it mediates the monocytic up-regulation of TNF-α, IL-1β, and IL-6 (46–48). As in the published literature, the inflammatory mediators, such as TNF-α, IL-1β, IFN-γ, and LPS, markedly enhance the production of activin A (49, 50). Here, our results clearly indicate that an LTA4H activator can act on monocytes to stimulate the production of LTB4, resulting in B-cell proliferation and an increase of Ig production by serial production of autocrine signal mediators, such as TNF-α, activin A, and paracrine BAFF. A schematic representation of the proposed mechanism of action of P_4N is presented in Fig. 7.

GRP78 is an endoplasmic reticulum chaperone that facilitates protein assembly and regulates endoplasmic reticulum stress signaling. GRP78 resides not only in the endoplasmic reticulum but also in the nucleus and cytoplasm (51). During the integrated stress response, the phosphorylation of eukaryotic initiation factor 2α (eIF2α) catalyzes translation initiation of GRP78 at the UUG and CUG start codons in its 5′-untranslated region upstream ORFs (52). In malignant cells, GRP78 can translocate to the outside of the endoplasmic reticulum and to the cell surface (53, 54). Increased levels of surface GRP78 in cancer cells are correlated with tumor progression, angiogenesis, and metastasis (53–55). For CRC therapy, GRP78 silencing down-regulates the VEGF/VEGF receptor 2 pathway and suppresses human colon cancer tumor growth (55). Furthermore, a natural IgM anti-GRP78

antibody, PAT-SM6, isolated from the sera of patients with cancer can specifically recognize the surface GRP78 and induce apoptosis to inhibit tumor growth (9, 10). However, the natural GRP78 IgM has a low binding affinity and a restricted binding repertoire. To resolve this problem, a monoclonal anti-GRP78 antibody, mAb159, has been developed, and it can inhibit tumor growth and metastasis by modulating the PI3K pathway (56).

The other antigen, F1F0 ATP synthase, generally localizes to the mitochondrial inner membrane and converts ADP to ATP in the process of mitochondrial oxidative phosphorylation. In cancer cells, cell surface-translocated F1F0 ATP synthases have been identified that promote tumor cell survival and develop an acidic microenvironment in tumor tissues through shear stress stimulation-induced ATP and H(+) corelease and CO_2 gas production (57). Specific targeting of F1F0 ATP synthase by anti-ATP synthase β antibody led to the inhibition of cell proliferation (58). In this study, we show the potential of an antitumor drug, P_4N, converting inefficient EAAs against cell surface GRP78 and F1F0 ATP synthase into more efficient treatment modalities.

Patients with cancers other than CRC have been proven to generate autoantibodies in their sera that recognize their own tumor antigens (2). However, these EAAs do not provide a therapeutic benefit for tumor elimination, and can even facilitate tumor growth. Passive transfer of antitumor antibodies offers a more efficient therapeutic modality. For example, a humanized monoclonal anti-GPR78 antibody (mAb159) that has shown inhibitory activity for CRC (56) has been developed. Patients with normal immunity who have cancer may negatively select out B cells with high activities against autoantigens, resulting in low-activity EAAs. Although the process of somatic hypermutation can raise the activities of EAAs from low to high, the interaction of CD40 ligand of $CD4^+$ T cells with CD40 on B cells to induce AID expression is necessary for this process. The autoreactive $CD4^+$ T cells, however, will be depleted during T-cell development in the thymus by negative selection. In contrast, clinical target antibodies are artificially selected and produced, and their titers and activities can be raised by modern biotechniques, resulting in more efficient therapeutic effects. In vivo amelioration of EAAs is difficult, but we have shown that amelioration can be accomplished with low-dose P_4N.

The breadth and potency of P_4N's effect have not been fully addressed in this report. Our preliminary experiments show that i.v.-administered P_4N is able to shrink the size of tumor explants of OVCAR-8 human ovarian cancer cells and inhibit the growth of LN229 human glioma cell-derived tumors in nude mice (*SI Appendix*, Fig. S14). The mechanism of P_4N action in these cases, however, has not been determined. Whether the immune response elicited by P_4N is potent enough of itself to eradicate tumors is not clear. To achieve complete remission and cures for patients with cancer, combining anticancer therapies has proven essential. For many tumors, the combination of immunotherapy and chemotherapy is the standard of care (59). Immunomodulation with P_4N may ultimately be most effective when used in combination with other chemotherapeutic agents.

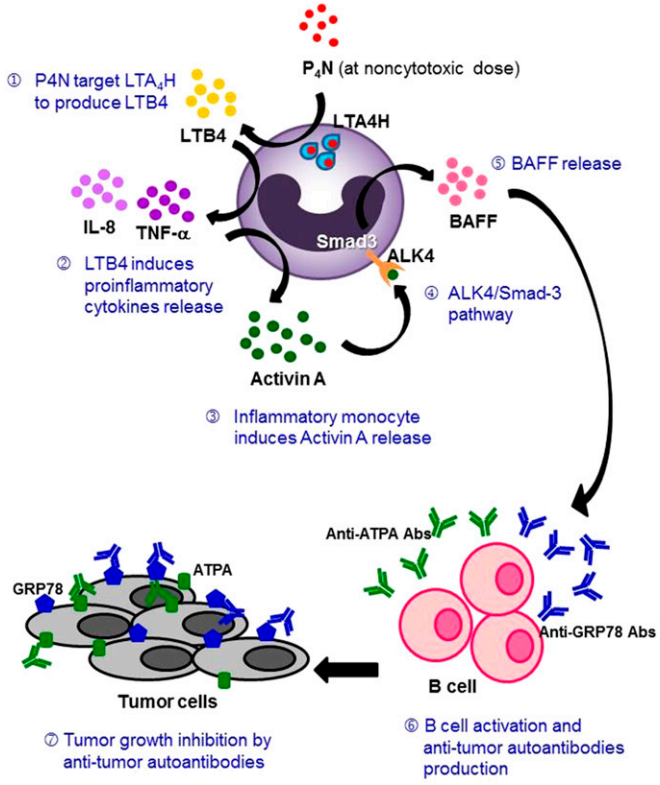

Fig. 7. Schematic representation of the proposed mechanism of action of P_4N.

Materials and Methods

Reagents. P_4N was synthesized from NDGA by the Hwu laboratory, Department of Chemistry, National Tsing Hua University and provided for this study by R.C.C.H. SB431542 (ALK4 inhibitor), SIS-3 (Smad3 inhibitor), SB203580 (p38 inhibitor), and PD98059 (MAPK/ERK inhibitor) were purchased from Sigma–Aldrich. A83-01 (ALK4 inhibitor) was procured from R&D Systems.

Cells. CT26 and THP-1 cells were purchased from the Bioresource Collection and Research Center. CT26 cells were maintained in RPMI-1640 culture medium (Invitrogen) supplemented with 10% (vol/vol) FCS (Invitrogen) and 1% penicillin/streptomycin (Invitrogen). THP-1 cells were maintained in RPMI-1640 supplemented with 4.5 g/L glucose, 10 mM Hepes, 1.0 mM sodium pyruvate, 0.05 mM 2-mercaptoethanol, 10% (vol/vol) FCS, and 1% penicillin/streptomycin.

PBMCs were isolated from the blood of healthy human donors by density separation over Lymphoprep (Axis-Shield). Mononuclear cells at the interface were carefully transferred into a centrifuge tube and then treated with ACK hemolysis buffer (0.15 M NH_4Cl, 10 mM $KHCO_3$, 0.1 mM Na_2EDTA), washed twice with PBS, and cultured in growth medium.

Total B cells were isolated from human PBMCs or mouse splenocytes by negative selection using a magnetic sorting device (Miltenyi Biotec). Briefly, PBMCs were incubated with a mixture of biotin-conjugated antibodies, followed by microbead-conjugated antibiotin antibodies for magnetic depletion. B cells were eluted according to the manufacturer's protocols. Human blood samples were collected from healthy individuals with their informed consent following an institutional review board (IRB)-approved protocol and in agreement with the Committee for Research Ethics Board of Chung Shan Medical University Hospital (IRB approved no. CS14047).

Animals. Female BALB/c and BALB/c/nude mice were purchased from The National Laboratory Animal Center and maintained on a 12:12-h light/dark cycle in an animal environmental control chamber (Micro-VENT IVC Systems). Humane animal care was ensured by use of the institutional guidelines of National Chiao Tung University (NCTU). The Committee on Animal Experimentation of the Center for Experimental Animals of the NCTU approved all studies and procedures.

P_4N Treatments in Vivo. BALB/c or BALB/c/nude mice (6 wk old) were inoculated s.c. with 1×10^6 CT26 cells in 100 μL of PBS. When the average tumor mass reached 50 mm^3, the animals were treated with 2.5 mg/kg or 5 mg/kg of P_4N in one intratumoral injection. Subsequently, the tumor volumes were measured using a caliper every 2 d, and the volumes were calculated using the following formula: volume (mm^3) = length × width × height. Before euthanasia, the sera of the mice were collected for experimental use.

In Vivo Cell Depletion. $CD8^+$ T and B cells were depleted by monoclonal antibodies following the protocol of Carmi et al. (60). $CD8^+$ T cells were depleted by i.p. injection of 500 μg of anti-CD8 (YST-169.4) monoclonal antibodies (BioXcell) per mouse 3 d before tumor inoculation and every 3 d thereafter. For B-cell depletion, 300 μg of anti-CD19 (1D3) and 300 μg of anti-220 (RA3.3A1/6.1) monoclonal antibodies (BioXcell) were i.p. injected per mouse 3 wk before tumor inoculation and every 5 d thereafter. Macrophages were depleted with liposomal clodronate. Briefly, mice were i.p. injected with 200 μL of liposomal clodronate for the first week and then injected with 100 μL of liposomal clodronate weekly. The extent of

depletion of CD8T, B cells, and macrophages was evaluated by IHC staining. Tumor tissue was randomly selected from depleted animals; embedded in paraffin; and probed with rat monoclonal anti-CD20, anti-CD8, and anti-F4/80 antibodies (results are shown in *SI Appendix*, Figs. S12 and S15).

Sera Transfer in Vivo. In a metastatic model, BALB/c mice were i.v. injected with 1×10^6 CT26 cells in 100 μL of PBS via the tail vein, and then treated with 100 μL of antisera once every week. Upon the death of the mice, the lungs were dissected, observed, and photographed. Three mice in the P_4N antisera group were killed 24 d after injection. Tumor nodules on the lungs were counted, and lung weights were determined. Survival of the mice was noted, and rates of survival were calculated. In an s.c. tumor model, the nude mice bearing ∼50-mm^3 CT26 tumors were injected i.v. with 100 μL of the different antisera once every week. The tumor volumes were measured as described above.

IHC Staining. Tumors isolated from P_4N- and vehicle-treated mice were embedded in paraffin, and thin sections were made and processed for IHC staining. The sections were probed with rat monoclonal anti-F4/80 (1:50 dilution; GeneTex) and anti-CD20 (1:200 dilution; Santa Cruz Biotechnology), hamster monoclonal anti-CD11c (1:25 dilution; GeneTex), rabbit monoclonal anti-CD3 (1:50 dilution; GeneTex), and rabbit polyclonal anti–TNF-α and anti–IL-8 antibodies (1:50 dilution; Assay BioTech) at 4 °C overnight, and the detection antibodies were recognized using a horseradish peroxidase (HRP)-conjugated anti-rat, anti-hamster, or anti-rabbit IgG antibody (1:1,500 dilution; Santa Cruz Biotechnology). The immune complexes in the sections were visualized using the LSAB2 System (DAKO). The sections were counterstained with hematoxylin, mounted, observed under a light microscope at a magnification of 400×, and photographed.

Sections of CT26 tumors from untreated mice were incubated with a 200-fold dilution of normal sera, PBS antisera, or P_4N antisera at 4 °C overnight. The sections were then incubated with an HRP-conjugated anti-mouse IgG antibody (1:1,500 dilution; Santa Cruz Biotechnology), developed, counterstained, and photographed as described above.

Titers and Ig Classes of Antitumor Autoantibodies. Blood was collected weekly from CT26-bearing mice treated with PBS or 5 mg/kg P_4N, and the titers of CT26-specific antibodies in the sera were measured by the following method. The wells of 96-well culture plates were seeded with CT26 (10^6 cells per well) or mouse mammary gland adenocarcinoma JC cells (10^6 cells per well). On the following day, the cells were fixed with 4% (wt/vol) paraformaldehyde, washed, and blocked with 300 μL of 2% (wt/vol) skim milk in PBST (PBS buffer with 0.05% Tween-20) for 1 h. One hundred microliters of 6,400-fold diluted sera in PBS containing 0.5% skim milk was loaded into each well and incubated at room temperature for 2 h. After washing three times, 100 μL of HRP-conjugated anti-mouse Ig antibody (1:10,000 dilution; Sigma–Aldrich) was added to each well and incubated for 1 h. After washing three times, 100 μL of NeA-Blue (Clinical Science Products, Inc.) was added to each well, incubated for 20 min, and stopped using 100 μL of 1-N HCl. The optical density was measured at 450 nm using an ELISA reader (Tecan). The isotypes of specific anti-CT26 cell antibodies in antisera (1:1,600 dilution) were determined by using HRP-conjugated specific anti-mouse IgM, IgG1, IgG2a, IgG2b, or IgA antibodies (Acris).

Immunofluorescence Analysis of Cell Surface Tumor Antigens. CT26 cells were seeded on glass cover slides, and fixed with 4% (wt/wt) paraformaldehyde The fixed cells were then incubated with normal sera, PBS antisera, or P_4N antisera for 1 h and detected with secondary antibodies conjugated to Alexa Fluor 568 (Molecular Probes). Alexa Fluor 488-conjugated Con A (Molecular Probes) and DAPI (Molecular Probes) were used to label the plasma membrane and nucleus, respectively. The images of tumor antigens recognized by the antisera were photographed at a magnification of 400× using a Zeiss LSM 510 META confocal microscope (Carl Zeiss).

Western Blot Analysis. The membrane proteins of 3×10^7 CT26 cells were extracted and harvested with the Mem-PER Eukaryotic Membrane Protein Extraction Reagent Kit (Thermo Fisher Scientific), following the manufacturer's instructions. Fifty micrograms of total membrane protein was subjected to SDS/PAGE; transferred to Nitrocellulose Blotting Membrane (General Electric); and probed with normal sera, PBS antisera, or P_4N antisera. The membranes were then blocked with 2% (wt/vol) milk in PBST, incubated with HRP-conjugated anti-mouse Ig antibody (1:10,000 dilution; Sigma–Aldrich), and developed with the WesternBright ECL Western blotting detection kit (Advansta). Antibody-bound proteins were visualized by the Hansor Luminescence Image System (Hansor). E-cadherin proteins in all samples were probed by rabbit polyclonal anti–E-cadherin antibody (1:1,000 dilution; GeneTex) and HRP-conjugated anti-rabbit Ig antibody (1:10,000 dilution; Sigma–Aldrich).

Co-Immunoprecipitation Assay. Five microliters of normal sera, PBS antisera, or P_4N antisera was mixed with 100 μL of protein G agarose (Merck Millipore), and then covalently linked with disuccinimidyl suberate (Thermo Fisher Scientific). After washing, 5 μL of protein G agarose-conjugated sera was incubated with 400 μL of membrane proteins at room temperature. The immune complexes were then washed three times with lysis buffer and eluted with elution buffer (Thermo Fisher Scientific). The precipitated samples were then heated in reducing sample buffer and resolved by the SDS/PAGE.

Antigen Identification by UPLC/HRMS/MS. Proteins were excised from SDS polyacrylamide gels, digested with the In-Gel Tryptic Digestion Kit (Thermo Fisher Scientific), and identified by UPLC/HRMS/MS (Bruker BioSpin). Peptide sequence information was used to search sequences in the protein database of the National Center for Biotechnology Information using BLAST (blast.ncbi.nlm.nih.gov/blast.cgi).

Cytokine Multiplex Assay. THP-1 cells (5×10^5 cells per milliliter) in 1 mL of culture medium were seeded in each well of a 24-well microplate and treated with 3 μM P_4N for 24 h. Cell culture supernatants were collected and analyzed by a cytokine multiplex assay following the Bio-Plex Pro Human Cytokine Standard Group I 27-Plex, according to the manufacturer's protocol (Bio-Rad). The change levels of cytokine were calculated as follows: Change level = (value of the P_4N-treated cells)/(value of the untreated cells) × 100%.

Gene Expression Profiling and Analysis. Amplification and labeling of RNA were performed with the IlluminaTotalPrep RNA Amplification Kit from Life Technologies (Ambion; Applied Biosystems) using 150 ng of RNA per sample. Labeled RNA (750 ng) was hybridized to Illumina HT-12 v4 Expression BeadChips (∼48,000 probes) and processed according to the manufacturer's protocol. Expression data underwent quality control and normalization by Genome Studio (Illumina). Genes differentially expressed in the cells treated with P_4N relative to the untreated cells were identified, with special emphasis given to genes involved in cytokine–cytokine receptor interaction (KEGG pathway). Genes with a P value <0.05 and a fold change ≥0.4 were considered to be differentially expressed, up-regulated genes. The identified genes were subjected to the Database for Annotation, Visualization, and Integrated Discovery (https://david.ncifcrf.gov/) for GO and KEGG pathway enrichment analysis. A P value <0.05 was set as the threshold of enrichment analysis.

RT-PCR. Human PBMCs or THP-1 cells were treated with P_4N, and the mRNA expression of activin A and *BAFF* in these cells was then measured by RT-PCR. Briefly, total cellular RNA was extracted with TRIzol reagent (Invitrogen) and reverse-transcribed into cDNA using the SuperScript RT-Kit (Invitrogen). The cDNA of activin A and BAFF was then amplified by PCR. The primers for human activin A were forward primer 5′-GCCGAGTCAGGAACAGCCAG-3′ and reverse primer 5′-TTTCTTCTTCTTCTTGCCCAGGA-3′, and the primers for human BAFF were forward primer 5′-ATGGATGACTCCACAGAAAGG-3′ and reverse primer 5′-TGGTAGAAAGACACCACCG-3′. All PCR reagents used to amplify the cDNA were purchased from Promega. *GAPDH* cDNA in the samples was used to normalize the loading amounts in each reaction. Finally, PCR products were resolved by electrophoresis on 2% agarose gels, stained with ethidium bromide, and photographed using the Uni-photo band tool (EZ laboratory).

Cell Proliferation Assay. Purified B cells (2×10^5 cells per well) were prestained with DiI fluorescent dye, seeded, and treated with THP-1–conditioned media. After 30 h, the number of viable cells was determined by flow cytometry.

Activin A and BAFF Neutralization. To examination the roles of activin A and BAFF involved in P_4N-induced B-cell proliferation, purified B cells (2×10^5 cells per well) were treated with P_4N-treated THP-1 media and/or 500 ng of neutralized anti-activin A antibody or anti-BAFF antibody for 30 h. Then, B-cell proliferation was determined as previously described.

ELISAs. THP-1 cells (1×10^6 cells per milliliter per well) in a 24-well culture plate were pretreated with 10 μM bestatin (LTA4H inhibitor; Sigma–Aldrich) for 2 h and then treated with 3 μM P_4N for various time intervals. The levels of LTB4 in the culture media were determined by the LTB4 ELISA Kit (Enzo Life Sciences). The amounts of TNF-α, IL-8, and activin A in the cultured media were measured in a similar manner.

Statistical Analyses. The results are presented as the mean ± SEM. The statistical significance was evaluated using Student's t test, and $P < 0.05$ was considered significant.

ACKNOWLEDGMENTS. We thank Prof. Jinn-Moon Yang for kind support in docking technology. We thank the core facility of the multiphoton and confocal microscope system and UPLC/HRMS/MS of the NCTU. This research was supported by Grants NCTU 102W976 and NCTU 103W976 (to R.C.C.H.) and Ministry of Science and Technology of Taiwan (MOST) Grants MOST 104-2627-M-009-007 and MOST 103-2112-M-009-011-MY3 (to C.C.C.).

1. International Agency for Research on Cancer, WHO (2015) GLOBOCAN 2012: Estimated Cancer Incidence, Mortality and Prevalence Worldwide in 2012. Available at globocan.iarc.fr/Default.aspx. Accessed August 10, 2015.
2. Chen H, Werner S, Tao S, Zörnig I, Brenner H (2014) Blood autoantibodies against tumor-associated antigens as biomarkers in early detection of colorectal cancer. *Cancer Lett* 346(2):178–187.
3. Babel I, et al. (2009) Identification of tumor-associated autoantigens for the diagnosis of colorectal cancer in serum using high density protein microarrays. *Mol Cell Proteomics* 8(10):2382–2395.
4. Ran Y, et al. (2008) Profiling tumor-associated autoantibodies for the detection of colon cancer. *Clin Cancer Res* 14(9):2696–2700.
5. Babel I, et al. (2009) Identification of tumor-associated autoantigens for the diagnosis of colorectal cancer in serum using high density protein microarrays. *Mol Cell Proteomics* 8(10):2382–2395.
6. Bei R, Masuelli L, Palumbo C, Modesti M, Modesti A (2009) A common repertoire of autoantibodies is shared by cancer and autoimmune disease patients: Inflammation in their induction and impact on tumor growth. *Cancer Lett* 281(1):8–23.
7. Zhang Y, Gallastegui N, Rosenblatt JD (2015) Regulatory B cells in anti-tumor immunity. *Int Immunol* 27(10):521–530.
8. Díaz-Zaragoza M, Hernández-Ávila R, Viedma-Rodríguez R, Arenas-Aranda D, Ostoa-Saloma P (2015) Natural and adaptive IgM antibodies in the recognition of tumor-associated antigens of breast cancer (Review). *Oncol Rep* 34(3):1106–1114.
9. Rasche L, et al. (2015) GRP78-directed immunotherapy in relapsed or refractory multiple myeloma - results from a phase 1 trial with the monoclonal immunoglobulin M antibody PAT-SM6. *Haematologica* 100(3):377–384.
10. Rasche L, et al. (2013) The natural human IgM antibody PAT-SM6 induces apoptosis in primary human multiple myeloma cells by targeting heat shock protein GRP78. *PLoS One* 8(5):e63414.
11. Oflazoglu E, Audoly LP (2010) Evolution of anti-CD20 monoclonal antibody therapeutics in oncology. *MAbs* 2(1):14–19.
12. Bianchini G, Gianni L (2014) The immune system and response to HER2-targeted treatment in breast cancer. *Lancet Oncol* 15(2):e58–e68.
13. Taylor RP, Lindorfer MA (2008) Immunotherapeutic mechanisms of anti-CD20 monoclonal antibodies. *Curr Opin Immunol* 20(4):444–449.
14. Selenko N, et al. (2001) CD20 antibody (C2B8)-induced apoptosis of lymphoma cells promotes phagocytosis by dendritic cells and cross-priming of CD8+ cytotoxic T cells. *Leukemia* 15(10):1619–1626.
15. He Q, et al. (2011) Low-dose paclitaxel enhances the anti-tumor efficacy of GM-CSF surface-modified whole-tumor-cell vaccine in mouse model of prostate cancer. *Cancer Immunol Immunother* 60(5):715–730.
16. Sevko A, et al. (2012) Application of paclitaxel in low non-cytotoxic doses supports vaccination with melanoma antigens in normal mice. *J Immunotoxicol* 9(3):275–281.
17. Zhong H, et al. (2007) Low-dose paclitaxel prior to intratumoral dendritic cell vaccine modulates intratumoral cytokine network and lung cancer growth. *Clin Cancer Res* 13(18 Pt 1):5455–5462.
18. Heylmann D, et al. (2013) Human CD4+CD25+ regulatory T cells are sensitive to low dose cyclophosphamide: Implications for the immune response. *PLoS One* 8(12):e83384.
19. Dimeloe S, et al. (2014) Human regulatory T cells lack the cyclophosphamide-extruding transporter ABCB1 and are more susceptible to cyclophosphamide-induced apoptosis. *Eur J Immunol* 44(12):3614–3620.
20. Lutz ER, et al. (2014) Immunotherapy converts nonimmunogenic pancreatic tumors into immunogenic foci of immune regulation. *Cancer Immunol Res* 2(7):616–631.
21. Sharabi A, Haran-Ghera N (2011) Immune recovery after cyclophosphamide treatment in multiple myeloma: Implication for maintenance immunotherapy. *Bone Marrow Res* 2011:269519.
22. Peng S, et al. (2013) Low-dose cyclophosphamide administered as daily or single dose enhances the antitumor effects of a therapeutic HPV vaccine. *Cancer Immunol Immunother* 62(1):171–182.
23. Sharabi A, Laronne-Bar-On A, Meshorer A, Haran-Ghera N (2010) Chemoimmunotherapy reduces the progression of multiple myeloma in a mouse model. *Cancer Prev Res (Phila)* 3(10):1265–1276.
24. Kaneno R, et al. (2011) Chemotherapeutic agents in low noncytotoxic concentrations increase immunogenicity of human colon cancer cells. *Cell Oncol (Dordr)* 34(2):97–106.
25. Shurin GV, Tourkova IL, Kaneno R, Shurin MR (2009) Chemotherapeutic agents in noncytotoxic concentrations increase antigen presentation by dendritic cells via an IL-12-dependent mechanism. *J Immunol* 183(1):137–144.
26. Kaneno R, Shurin GV, Tourkova IL, Shurin MR (2009) Chemomodulation of human dendritic cell function by antineoplastic agents in low noncytotoxic concentrations. *J Transl Med* 7:58.
27. Dohm JA, et al. (2005) Influence of ions, hydration, and the transcriptional inhibitor P_4N on the conformations of the Sp1 binding site. *J Mol Biol* 349(4):731–744.
28. Hwu JR, Hsu MH, Huang RC (2008) New nordihydroguaiaretic acid derivatives as anti-HIV agents. *Bioorg Med Chem Lett* 18(6):1884–1888.
29. Lü JM, et al. (2010) Molecular mechanisms and clinical applications of nordihydroguaiaretic acid (NDGA) and its derivatives: An update. *Med Sci Monit* 16(5):RA93–RA100.
30. Zhang Y, et al. (2012) mTORC1 is a target of nordihydroguaiaretic acid to prevent breast tumor growth in vitro and in vivo. *Breast Cancer Res Treat* 136(2):379–388.
31. Kim JH, Seo GY, Kim PH (2011) Activin A stimulates mouse APCs to express BAFF via ALK4-Smad3 pathway. *Immune Netw* 11(4):196–202.
32. Haeggström JZ (2004) Leukotriene A4 hydrolase/aminopeptidase, the gatekeeper of chemotactic leukotriene B4 biosynthesis. *J Biol Chem* 279(49):50639–50642.
33. Conti P, et al. (1993) Human recombinant IL-1 receptor antagonist (IL-1Ra) inhibits leukotriene B4 generation from human monocyte suspensions stimulated by lipopolysaccharide (LPS). *Clin Exp Immunol* 91(3):526–531.
34. Maloff BL, Fefer D, Cooke GM, Ackerman NR (1987) Inhibition of LTB4 binding to human neutrophils by nordihydroguaiaretic acid. *Agents Actions* 21(3-4):358–360.
35. Ogawa K, Funaba M, Tsujimoto M (2008) A dual role of activin A in regulating immunoglobulin production of B cells. *J Leukoc Biol* 83(6):1451–1458.
36. Hashimoto O, et al. (1998) The role of activin type I receptors in activin A-induced growth arrest and apoptosis in mouse B-cell hybridoma cells. *Cell Signal* 10(10):743–749.
37. Zipori D, Barda-Saad M (2001) Role of activin A in negative regulation of normal and tumor B lymphocytes. *J Leukoc Biol* 69(6):867–873.
38. Wang B, et al. (2009) Involvement of ERK, Bcl-2 family and caspase 3 in recombinant human activin A-induced apoptosis in A549. *Toxicology* 258(2-3):176–183.
39. Koseki T, et al. (1998) Correlation between Bcl-X expression and B-cell hybridoma apoptosis induced by activin A. *Cell Signal* 10(7):517–521.
40. Craxton A, Draves KE, Gruppi A, Clark EA (2005) BAFF regulates B cell survival by downregulating the BH3-only family member Bim via the ERK pathway. *J Exp Med* 202(10):1363–1374.
41. Anderson KS, et al. (2015) Autoantibody signature for the serologic detection of ovarian cancer. *J Proteome Res* 14(1):578–586.
42. Xu Z, et al. (2007) Regulation of aicda expression and AID activity: relevance to somatic hypermutation and class switch DNA recombination. *Crit Rev Immunol* 27(4):367–397.
43. Stavnezer J, Schrader CE (2014) IgH chain class switch recombination: Mechanism and regulation. *J Immunol* 193(11):5370–5378.
44. Muramatsu M, et al. (2000) Class switch recombination and hypermutation require activation-induced cytidine deaminase (AID), a potential RNA editing enzyme. *Cell* 102(5):553–563.
45. Lee HJ, Seo GY, Kim HA, Kim PH (2008) Activin A stimulates IgA expression in mouse B cells. *Biochem Biophys Res Commun* 366(2):574–578.
46. Rola-Pleszczynski M, Lemaire I (1985) Leukotrienes augment interleukin 1 production by human monocytes. *J Immunol* 135(6):3958–3961.
47. Poubelle PE, Stankova J, Grassi J, Rola-Pleszczynski M (1991) Leukotriene B4 up-regulates IL-6 rather than IL-1 synthesis in human monocytes. *Agents Actions* 34(1-2):42–45.
48. Xu S, Lu H, Lin J, Chen Z, Jiang D (2010) Regulation of TNFalpha and IL1beta in rheumatoid arthritis synovial fibroblasts by leukotriene B4. *Rheumatol Int* 30(9):1183–1189.
49. Yoshino O, et al. (2011) Activin-A is induced by interleukin-1β and tumor necrosis factor-α and enhances the mRNA expression of interleukin-6 and protease-activated receptor-2 and proliferation of stromal cells from endometrioma. *Fertil Steril* 96(1):118–121.
50. Jones KL, et al. (2007) Activin A is a critical component of the inflammatory response, and its binding protein, follistatin, reduces mortality in endotoxemia. *Proc Natl Acad Sci USA* 104(41):16239–16244.
51. Ni M, Zhang Y, Lee AS (2011) Beyond the endoplasmic reticulum: Atypical GRP78 in cell viability, signalling and therapeutic targeting. *Biochem J* 434(2):181–188.
52. Starck SR, et al. (2016) Translation from the 5′ untranslated region shapes the integrated stress response. *Science* 351(6272):aad3867.
53. Yao X, et al. (2015) Cell surface GRP78 accelerated breast cancer cell proliferation and migration by activating STAT3. *PLoS One* 10(5):e0125634.
54. Li Z, et al. (2013) Cell-surface GRP78 facilitates colorectal cancer cell migration and invasion. *Int J Biochem Cell Biol* 45(5):987–994.
55. Kuo LJ, Hung CS, Chen WY, Chang YJ, Wei PL (2013) Glucose-regulated protein 78 silencing down-regulates vascular endothelial growth factor/vascular endothelial growth factor receptor 2 pathway to suppress human colon cancer tumor growth. *J Surg Res* 185(1):264–272.
56. Liu R, et al. (2013) Monoclonal antibody against cell surface GRP78 as a novel agent in suppressing PI3K/AKT signaling, tumor growth, and metastasis. *Clin Cancer Res* 19(24):6802–6811.
57. Kawai Y, Kaidoh M, Yokoyama Y, Ohhashi T (2013) Cell surface F1/FO ATP synthase contributes to interstitial flow-mediated development of the acidic microenvironment in tumor tissues. *Am J Physiol Cell Physiol* 305(11):C1139–C1150.
58. Fliedner SM, et al. (2015) Potential therapeutic target for malignant paragangliomas: ATP synthase on the surface of paraganglioma cells. *Am J Cancer Res* 5(4):1558–1570.
59. Mahoney KM, Rennert PD, Freeman GJ (2015) Combination cancer immunotherapy and new immunomodulatory targets. *Nat Rev Drug Discov* 14(8):561–584.
60. Carmi Y, et al. (2015) Allogeneic IgG combined with dendritic cell stimuli induce antitumour T-cell immunity. *Nature* 521(7550):99–104.